In-situ structural investigation of amorphous and nanocrystalline $Fe_{40}Co_{38}Mo_4B_{18}$ microwires.

S. Michalik[1,2*], J. Gamcová[1,2], J. Bednarčík[2], Varga[1]

[1] Institute of Physics, P.J. Šafárik University in Košice, Park Angelinum 9, 041 54 Košice, Slovakia

[2] Deutsches Elektronen Synchrotron DESY, Notkestrasse 85, D-22603 Hamburg, Germany

Abstract

Thermal evolution of the structure of glass-coated nanocrystalline FeCoMoB microwire during its devitrification has been studied. It is shown that annealing at the temperature above 411 ^{o}C leads to the formation of crystalline α-FeCo grains with diameter ~ 12 nm. Annealing at higher temperature increases the crystalline weight fraction up to 40% at 565 ^{o}C. However, crystalline grains size increases very weakly to ~ 13 nm. The thermal expansion coefficient of nanocrystalline microwire decreases by one half comparing to that of the amorphous precursor.

Key word: A. metallic glasses (microwires), C. microstructure, D. X-ray diffraction

1. Introduction

Nanocrystalline glass-coated microwires become a new class of material very promising for applications due to their excellent combination of soft magnetic properties and stability of nanocrystalline materials with small dimensions, circular symmetry and insulating glass-coating of magnetic microwires [1-4].

* Corresponding authors, Tel.: +421 055 234 6127; fax: +421 55 792 2408
E-mail: Stefan.michalik@upjs.sk

Nanocrystalline soft magnetic materials are composites that consist of crystalline grains of few nm in diameter (typically ~ 10 nm) embedded in amorphous matrix [5]. They are prepared by controlled thermal treatment of amorphous precursor. Since the crystallographic orientation of the grains is random, the magnetocrystalline anisotropy is averaged out. Due to their dimensions (that are much smaller than the exchange interaction length L_{ex} ~ 35-45 nm), their easy axis is finally given by the exchange interaction between crystalline grains through the amorphous matrix.

Amorphous glass-coated microwires (as a precursors for nanocrystalline microwires) are composite materials that consist of metallic nucleus (of diameter 0.5-40 μm) and glass-coating (thickness of 2-20 μm) [6, 7]. They are prepared by drawing and quenching of master alloys by Taylor Ulitovsky method. Since there is no crystalline structure, the most important anisotropies that control the magnetic properties are magnetoelastic and shape anisotropy. Finally, the domain structure of microwire with positive magnetostriction consists of single axial domain in the centre of the wire that is surrounded by the radial domain structure [8]. Such domain structure results in magnetic bistability (e.g. magnetization can have only two values: $-M_s$ and M_s; being M_s the saturation magnetization). Moreover, the magnetization process that is governed by a single Barkhaussen jump when the applied field approaches the switching field. The switching field is sensitive to the external parameters (temperature, stress, etc.) what makes the microwire ideal material for sensing application.

Combination of nanocrystalline structure and glass-coated microwire leads to a very interesting material that is structurally very stable and magnetically very soft [1, 2]. However, glass-coating introduces additional stresses during thermal treatment that sometimes results in the appearance of new non-magnetic phases (γ-Fe) [9,10]. Hence, new classes of nanocrystalline microwires FeNiMoB and FeCoMoB has been developed to avoid such a problem [1,2].

Moreover, nanocrystalline FeCoMoB microwire is characterized by a high Curie temperature and high magnetization – properties necessary for high temperature applications. Surprisingly, its magnetic softness is not influenced by heat treatment within a wide range of temperatures (450-600^{o}C). The aim of this work was to study the evolution of nanocrystalline structure of FeCoMoB glass-coated

microwires during the heat treatment in order to explain their unusual magnetic stability when they are heat treated in a quite wide range of temperatures.

2. Experimental details

The in-situ X-ray diffraction (XRD) experiments were carried out with the multipurpose diffraction instrument at the high-energy beamline BW5 of the DORIS III positron storage ring operated by DESY/HASYLAB (Hamburg, Germany). A bunch of FeCoMoB microwires was put into a quartz capillary having a diameter of 2 mm. Annealing was performed using a two-lamp infrared furnace. The sample temperature was controlled by a thermocouple positioned in the vicinity of the sample. Capillary containing the sample was instantaneously pumped down using a turbo molecular pump so that the vacuum was better than 10^{-4} mbar. In-situ experiment started with annealing of a sample up to 200 °C with the heating rate of 50 °C/min. Heating rate was slowed down to 5 °C/min for the temperature interval 200 – 565 °C. A series of XRD patterns was recorded during such temperature profile. It should be noted here that two experimental points have been lost due to the electron beam injection in the storage ring during realization of the in-situ experiment. XRD experiments were done in a transmission mode using a monochromatic photon beam with the energy of 100 keV (λ = 0.1239 Å). The sample material was illuminated for 100 s by an incident beam having the cross section of 1×1 mm^2. Diffracted photons were collected using an image plate detector MAR345 (2300×2300 pixels, pixel size 150×150 μm^2). Sample to detector distance, detector orthogonality with respect to the incoming radiation, as well as the instrumental broadening were determined by fitting a standard reference LaB_6 specimen. Obtained two-dimensional XRD patterns were integrated using a FIT2D program [11].

Theory

In our work we start from results presented by P. Riello et al. [12] in which they introduced a technique that allows an evaluation of the weight fraction of an amorphous phase from the total scattered intensity in the situation when the global chemical composition of the specimen and the

composition of all existing crystalline phases in the amorphous matrix are known. No information about chemical composition of the residual amorphous matrix is necessary and no external or internal standards are used. According the work of P. Riello et al. [12] (namely equations (4) and (4b) presented there) the weight fraction of the formed crystalline compound X_{crys} can be written using a following formula:

$$X_{crys} = \frac{\int_0^{\infty} \frac{Y_{crys}}{AP}(s)s^2 ds}{\sum_{i=1}^{n_{crys}} \int_0^{\infty} [|\ f_i^{\,0}(s)\,|^2 + I_i^{inc}(s)]s^2 ds} \Big/ \frac{\int_0^{\infty} \frac{Y_{total}}{AP}(s)s^2 ds}{\sum_{i=1}^{n_{sample}} \int_0^{\infty} [|\ f_i^{\,0}(s)\,|^2 + I_i^{inc}(s)]s^2 ds} \cdot \frac{\sum_{i=1}^{n_{crys}} w_i}{\sum_{i=1}^{n_{sample}} w_i} \qquad (1)$$

where $s = \sin(\theta)/\lambda$ and θ is the scattering angle. Y_{crys} is the intensity contribution of the crystalline phase to the global intensity of the XRD pattern Y_{total}. Actually Y_{total} was corrected for air scattering and as well as for contribution coming from the quartz capillary (see figure 1). *A* and *P* are correction factors for absorption and polarization. Due to the fact, that we used high energy synchrotron radiation these corrections are negligible. $f_i^{\,0}(s)$ is the tabulated atomic scattering factor of the *i*-th atom [13] and $I_i^{inc}(s)$ is the incoherent scattering of *i*-th atom calculated using Balyuzi formula [14]. n_{crys} and n_{sample} remark the number of atoms in the unit cell of the crystalline phase and the number of atoms in the composition unit of the sample, respectively. w_i is the atomic weight of the *i*-th atom. Every summation is evaluated on the relative stoichiometry. Finally the weight fraction of the amorphous phase X_{am} is estimated as $X_{am} = 1 - X_{crys}$.

The critical point of such analysis is reasonable separation of the amorphous and the crystalline contribution to the total scattering. We realized the profile fitting in the following way. The crystalline contribution Y_{crys} was expressed as a summation of four independent Gaussian functions $G_i(2\theta) = A_i \exp\left[-\ln(2)\frac{2\theta - 2\theta_i}{h_i}\right]$, A_i, $2\theta_i$ and $2h_i$ are the amplitude, the peak-maximum position and the full width at half maximum of the *i*-th peak. Four Bragg peaks stemming from cubic α–FeCo phase, namely (110), (200), (211) and (220), were included in the profile fitting analysis.

Furthermore XRD patterns acquired between temperatures 395 and 565 °C were analyzed. The amorphous part was described using the scattering of a pure amorphous material, Y_{am}, multiplied with a refined scaling factor C. For this purpose we used the diffraction profile of the $Fe_{40}Co_{38}Mo_4B_{18}$ microwires obtained at the temperature 380 °C. In order to deal up with some possible imperfection caused by subtraction of air and the capillary contribution to Y_{total}, the background function $B(2\theta)$ represented by second order polynomial was refined as well. Before applying equation (1) the background contribution was subtracted from Y_{total}. The total scattering intensity can be expressed as

$$Y_{total}(2\theta) = Y_{crys}(2\theta) + CY_{am}(2\theta) + B(2\theta) \qquad (2)$$

In the process of nonlinear curve fitting, the function $\left[Y_{total}(2\theta) - Y_{crys}(2\theta) + CY_{am}(2\theta) + B(2\theta)\right]^2$ was minimized and totally 16 parameters were refined.

3. Results and discussion

Figure 1 shows XRD pattern of the as-prepared FeCoMoB microwire before and after background subtraction due to air and the quartz capillary scattering. This background signal was obtained by measuring empty capillary using the same conditions as for the sample. Obtained XRD pattern reveals diffuse character indicating completely amorphous state of the as-prepared microwires. The pattern can be characterized with the dominant broad maximum positioned at $2\theta \sim 3.5°$ and one small maximum at 5.9°. Less intense diffuse peak located at 1.75° (see arrow in fig. 1) originates from the scattering of photons on the Pyrex-like glass which is actually covering microwires.

Since the glass-coated microwires are composite materials, it is quite difficult to measure the thermal expansion coefficient of metallic nucleus that finally determines the stress applied on it by glass-coating. However, using the below-described X-ray technique, the thermal expansion coefficient can be estimated very precisely. Figure 2 displays series of XRD profiles taken during in-situ measurement of the amorphous $Fe_{40}Co_{38}Mo_4B_{18}$ microwires. Amorphous state is maintained up to 411 °C when the first Bragg peaks are observed. At the first glance XRD patterns look the same however careful analysis reveals slight differences. Yavari et al. [15] showed that tracing the position

of the principal diffraction peaks with the temperature could be used for quantitative analysis of the volume changes:

$$\left\{\frac{s_{\max}(T_0)}{s_{\max}(T)}\right\}^3 = \frac{V(T)}{V(T_0)} = 1 + \alpha_{th}(T - T_0), \qquad (3)$$

where α_{th} is the volume coefficient of the thermal expansion of the amorphous phase below the glass temperature T_g and corresponds to the temperature slope or derivative of the reduced mean atomic volume $V(T)/ V(T_0)$ at T with reference T_0 corresponding to the room temperature. The profile of the main diffraction peak was fitted by Pseudo-Voigt function. As can be seen from figure 3 the reduced mean atomic volume linearly increases with temperature up to 335 °C. The thermal expansion coefficient was calculated from the slope of volume changes. Its value is $\alpha_{th} = (3.10 \pm 0.35) \times 10^{-5}\ 1/°\mathrm{C}$. Small minimum around 350 °C may be connected with the presence of the glass transition temperature T_g.

Crystallization of the FeCoMoB microwires starts at the temperature 411 °C when the first Bragg reflections stemming from the cubic α–FeCo phase (#PDF 441433, JCPDS PDF2 database [16]) are observed.. Further increase of the temperature leads to the increase of the intensity of Bragg peaks thus indicating an enhancement of the crystalline fraction in the amorphous matrix. In order to quantitatively follow this phase transformation the separation of contributions to the total intensity coming from the identified crystalline phase α-FeCo and the residual amorphous matrix was performed. The crystallinity degree was determined applying equation (1). Regarding the fact, that the weakly intense maximum located in the the 2θ-interval from 1.2° to 2.3° includes mainly scattering from the Pyrex-glass cover of microwires, this 2θ-interval was excluded from the profile fitting procedure. Figure 4 demonstrates the fitting results for a one selected XRD pattern (taken at 472 °C). One can observe that the crystalline and amorphous parts are clearly distinguishable. It follows from the fig. 5 that the amount of the crystalline α-FeCo phase is monotonously increasing with the temperature until it reaches about 40 % of the sample weight at 565 ^{o}C. As it will be shown bellow, the increase of crystalline phase volume is a result of nucleation of new grains rather than existing grain growth.

Fitting the profiles of the Bragg peaks above the first crystallization event yields information about peak positions and widths which were subsequently utilized to calculate the lattice parameter *a* and the average crystalline size *D* of the cubic α-FeCo phase. For calculation of the crystalline size the well-know Scherrer formula [17] was applied. Curves presented in fig. 6 indicate that α-FeCo nanoparticles have the average grain size between 11 and 13 nm. Moreover, it seems that their size is stable in relatively large temperature interval between 411 and 565 ^{o}C. It confirms the above mentioned fact that increase of the crystalline volume with increasing temperature is a result of nucleation of new grains rather than existing grain growth. Such a process leads to the creation of very fine nanocrystalline structure with a random distribution of easy magnetization axis in crystalline grains that finally leads to the averaging out of magnetocrystalline anisotropy.

The lattice parameter *a* of the cubic α-FeCo phase initially decreases and after reaching 470 °C it monotonously increases, most probably due to thermal expansion (figure 6). Thermal expansion coefficient of crystalline α-FeCo phase was estimated to be almost half of that of amorphous phase, see figure 7.

Klein at al. [1] have shown that the switching field in nanocrystalline FeCoMoB microwire is constant after the thermal treatment in the temperature interval between 425 °C and 600 °C. On the other hand it was proven that the magnetostriction of FeCoMoB alloys increases after nanocrystallization [18]. Hence, low stresses (introduced by low thermal expansion coefficient, as we show here) can be reason for the invariance of the switching field with annealing temperature.

4. Conclusions

We have studied the thermal evolution of microstructure of amorphous and nanocrystalline FeCoMoB glass-coated microwire. It was shown, that annealing above 411 ^{o}C leads to the formation of nanocrystalline structure with α-FeCo crystalline grains embedded in amorphous matrix. The grain size of crystalline phase is slightly above 11 nm and increases very smoothly up to 13 nm with the annealing temperature. The crystalline volume fracture increases slowly from 25% at 460 ^{o}C up to 40% at 565 ^{o}C. These results can explain unusual invariability of soft magnetic properties of nanocrystalline FeCoMoB microwire on the annealing temperature in a wide range of annealing

temperatures (425-600 ^{o}C) [1]. Moreover, we have demonstrated that x-ray diffraction utilizing high-energy photons is helpful tool for describing the thermal expansion of amorphous microwires. Having such a tool one may monitor the structural state of the metallic nucleus which is responsible for the overall soft magnetic properties of glass-coated microwires.

Acknowledgement

HASYLAB/DESY is gratefully acknowledged for the support during synchrotron beam time. S.M. thanks Deutscher Akademischer Austausch Dienst for providing the DAAD fellowship. J.G. acknowledge DESY for supplying the scholarship. We acknowledge prof. M. Vazquez from ICMM SCIC, Madrid for kindly supplying the samples. This work was supported by the scientific grants NanoCEXmat Nr. ITMS 26220120019, VEGA 1/0076/09 and VEGA 1/0167/10.

References

[1] P. Klein, R. Varga, P. Vojtanik, J. Kovac, J. Ziman, G. A. Badini-Confalonieri, M. Vazquez, J. Phys. D: Appl. Phys. 43 (2010) 045002.

[2] E. Komova, M. Varga, R. Varga, P. Vojtanik, J. Bednarcik, J. Kovac, M. Provencio, M. Vázquez, Appl. Phys. Lett. 93 (2008) 062502.

[3] H. Chiriac, M. Tibu, T.A. Ovari, IEEE Trans. Magn. 45 (2009) 4286-4289.

[4] J. Gonzalez, A. Zhukov, V. Zhukova, A.F. Cobeno, J.M. Blanco, A.R. de Arellano-Lopez, S. Lopez-Pombero, J. Martinez-Fernandez, V. Larin, A. Torcunov: IEEE Trans. Magn. 36**,** (2000) 3015.

[5] G. Herzer, IEEE Trans. Magn. 26 (5) 1990 1397.

[6] M. Vázquez, Handbook of Magnetism and Advanced Magnetic Materials: Advanced Magnetic Microwires, in H. Kronmüller, S. Parkin (Eds.), John Wiley & Sons, Chichester, UK 2007, pp. 2193-2226.

[7] A. Zhukov, J. Gonzalez, M. Vázquez, V. Larin, A. Torcunov, Encyclopedia of Nanoscience and Nanotechnology: Nanocrystalline and amorphous magnetic microwires, in H. S. Nalwa (Eds.) New York: American Scientific (2004) ch. 62, p. 23.

[8] H. Chiriac, T. A. Óvari, Prog. Mater. Sci. 40 (1996) 333.

[9] J. Gonzalez, A. Zhukov, V. Zhukova, A. F. Cobeno, J. M. Blanco, A. R. de Arellano-Lopez, S. Polez-Pombero, J. Martinez-Fernandez, V. Larin, A. Torcunov, IEEE Trans. Magn. 36 (2000) 3015.

[10] R. Varga, C. Luna, A. Zhukov, M. Vazquez, P. Vojtanik, Czech J. Phys. 54 Suppl. D. (2004), D177

[11] A. P. Hammersley, S. O. Svensson, M. Hanfland, A. N. Fitch, D. Häusermann, High Press. Res., Vol. 14 (1996) p. 235.

[12] P. Riello, P. Canton, G. Fagherazzi, J. Appl. Cryst. 31 (1998) 78-82.

[13] D. Waasmaier, A. Kirfel Acta Cryst. A 51, (1995) 413-416.

[14] H. H. M. Balyuzi, Acta Cryst. A 31 (1975) 600.

[15] A. R. Yavari, A. L. Moulec, A. Inoue, N. Nishiyama, N. Lupu, E. Matsubara, W.J. Botta, G. Vaughan, M. D. Michiel, A. Kvick, Acta Materialia 53 (2005) 1611-1619.

[16] JCPDS-ICDD, PCPDFWIN, 1998 (version 2.0).

[17] P. Scherrer, Göttinger Nachrichten Gesell. 2 (1918) 98.

[18] G. Vlasák, M. Pavúk, P. Mrafko, D. Janičkovič, P. Švec, B. Butvinova, J. Magn. Magn. Mater 320 (2008) 837

Fig. Captions

Figure 1. (Colour online) XRD patterns of as-prepared $Fe_{40}Co_{38}Mo_4B_{18}$ microwires before (top curve) and after (bottom curve) applying correction for air and quartz capillary scattering (dashed line).

Figure 2. (Colour online) Series of XRD patterns acquired during constant-rate heating (5 °C/min) of $Fe_{40}Co_{38}Mo_4B_{18}$ microwires. Miller indexes of four major Bragg reflections belonging to α-CoFe phase are depicted as well.

Figure 3. (Color online) Relative volume changes of $Fe_{40}Co_{38}Mo_4B_{18}$ microwires in amorphous state.

Figure 4. (Colour online) Comparison of the experimental XRD data (cross line) of $Fe_{40}Co_{38}Mo_4B_{18}$ microwires taken at 472 °C and the best-fit model (solid line) making a joint use of the amorphous (dot-dashed line) and crystalline (dashed line) part. In the bottom the difference curve is shown. Rwp is the weighted profile R-factor.

Figure 5. The weight fraction of α-CoFe phase during the crystallization process of $Fe_{40}Co_{38}Mo_4B_{18}$ microwires.

Figure 6. (Colour online) The average crystalline size (squares and left axis) and the lattice parameter *a* (stars and right axis) of α-CoFe phase during the crystallization process of $Fe_{40}Co_{38}Mo_4B_{18}$ microwires.

Figure 7 (Colour online) Relative volume changes of the α-CoFe phase identified during crystallization.

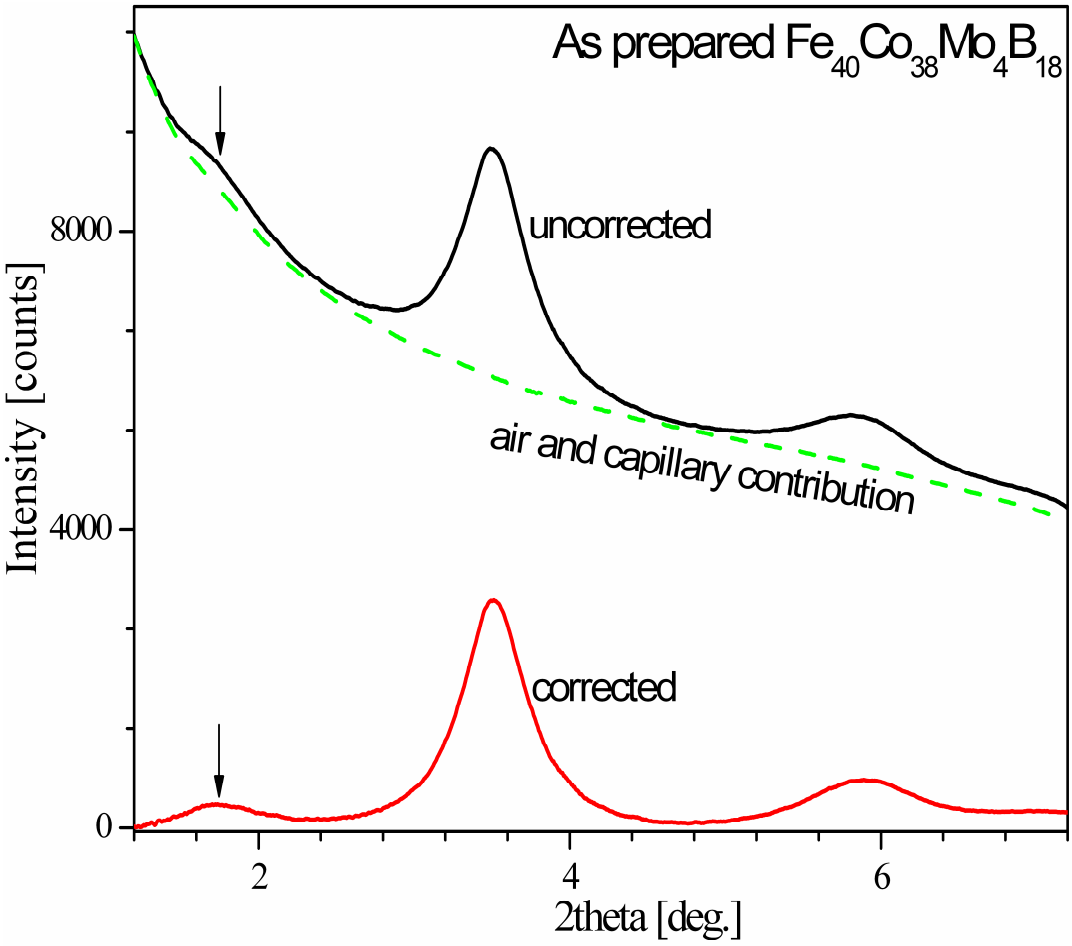

Figure 1, Michalik et al.

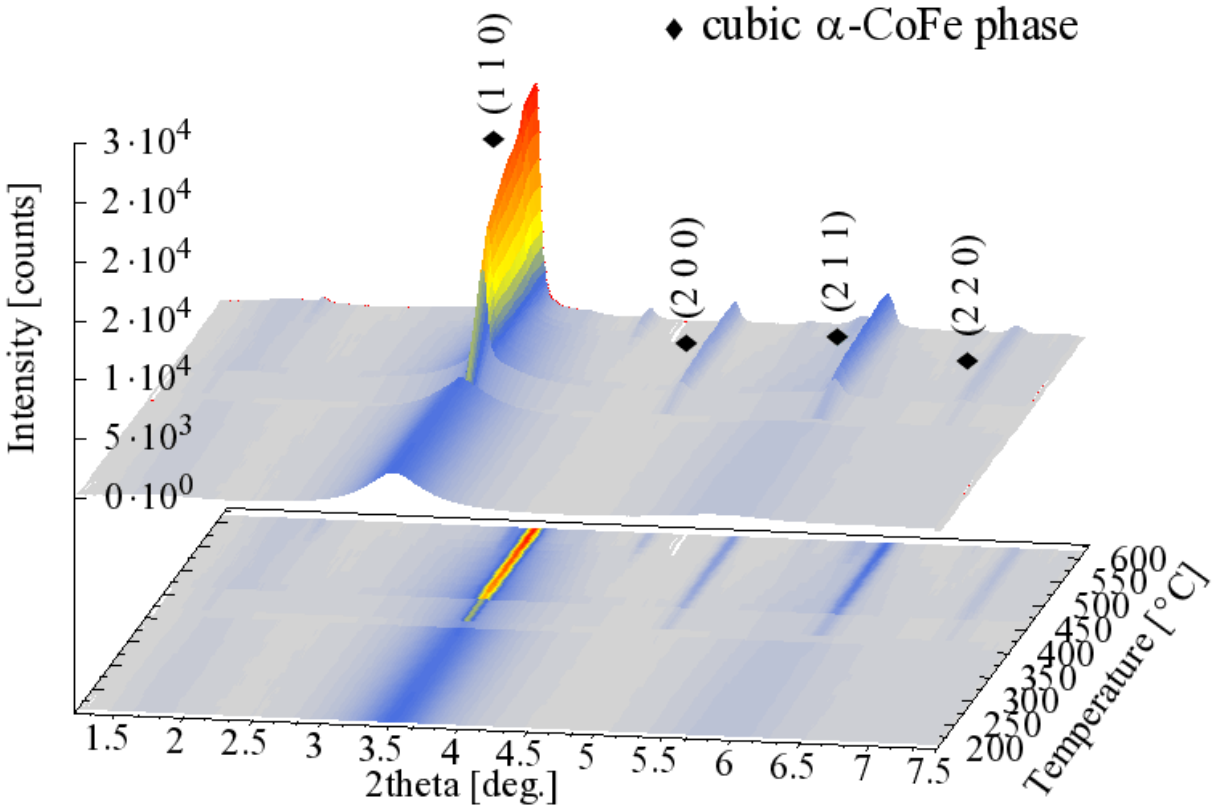

Figure 2, Michalik et al.

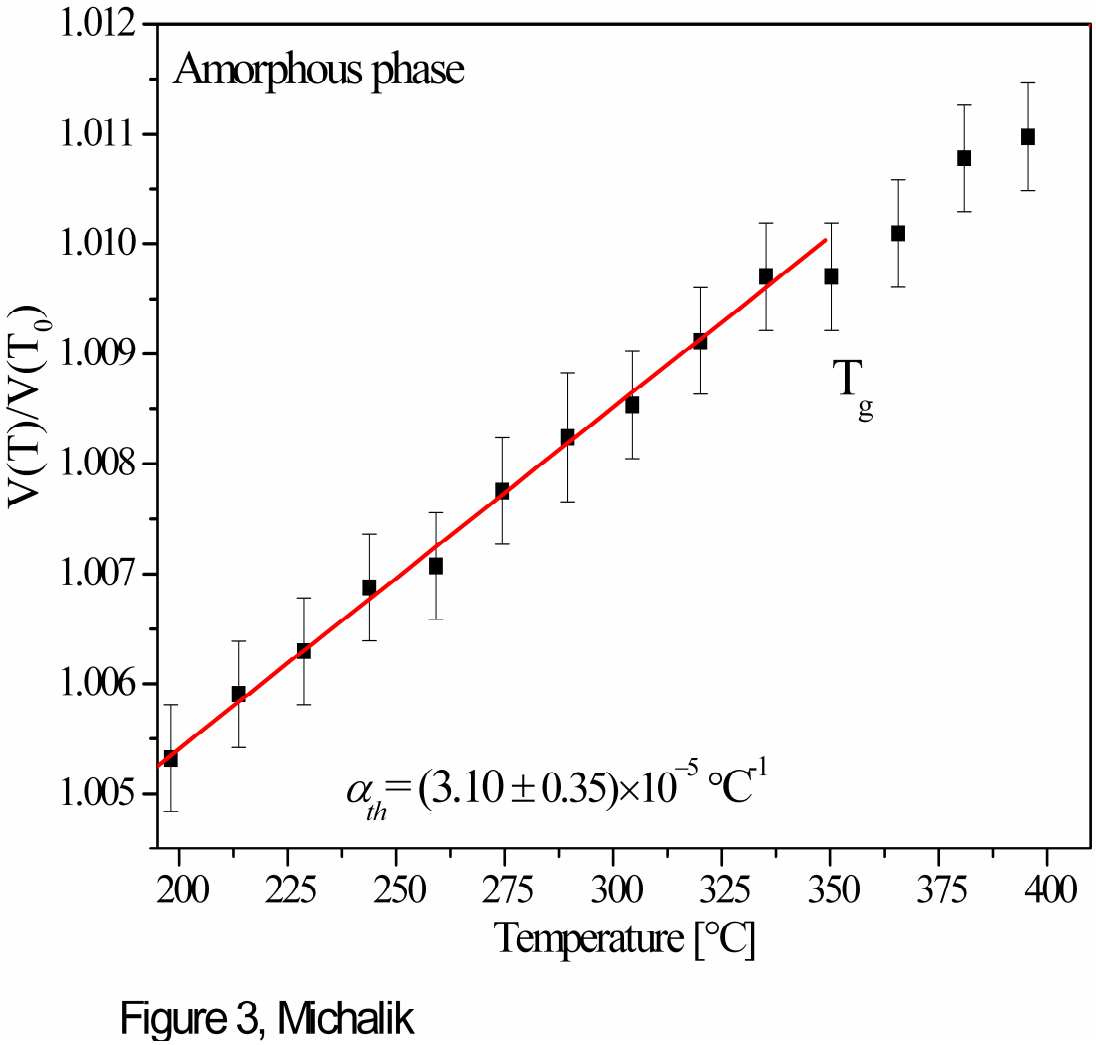

Figure 3, Michalik

Figure 4, Michalik

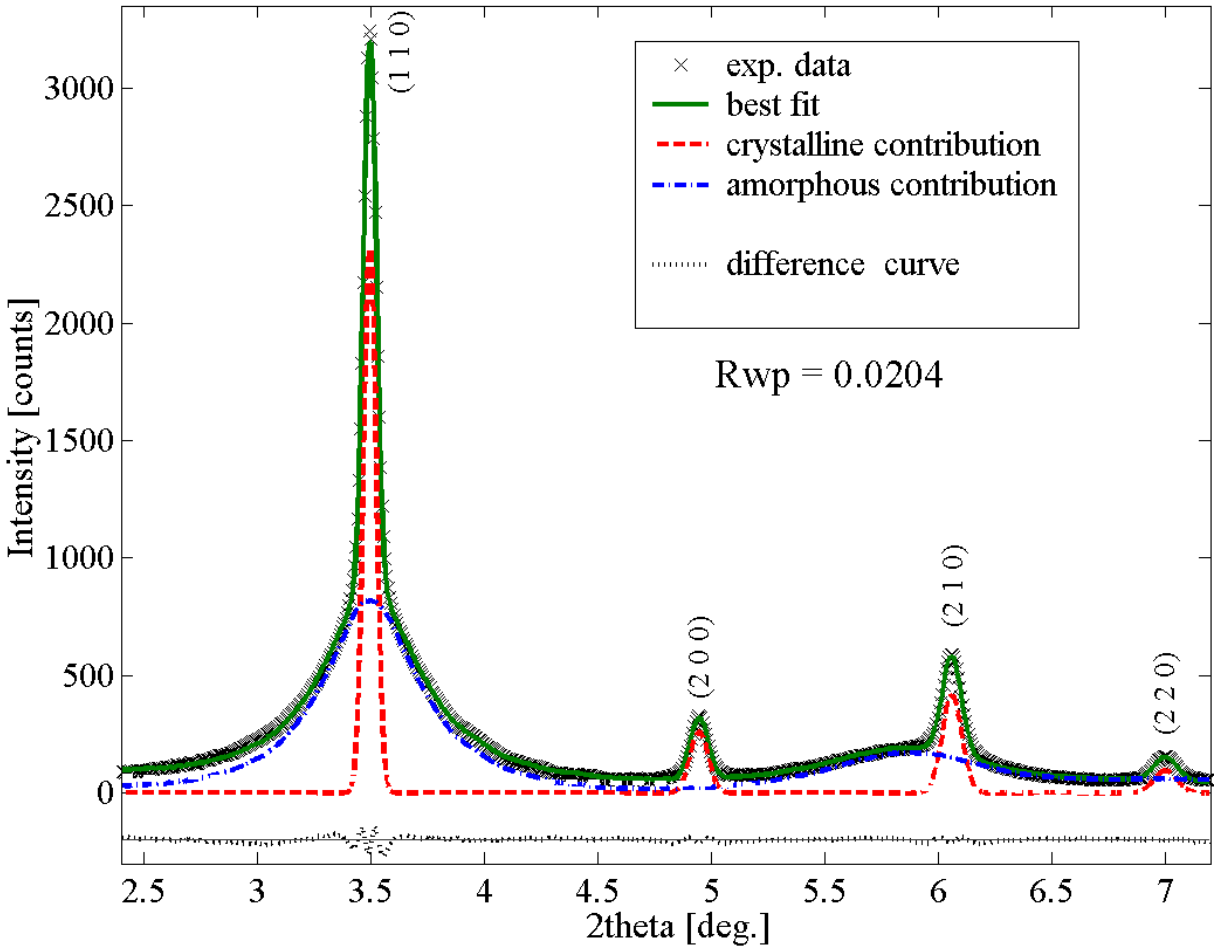

Figure 5, Michalik

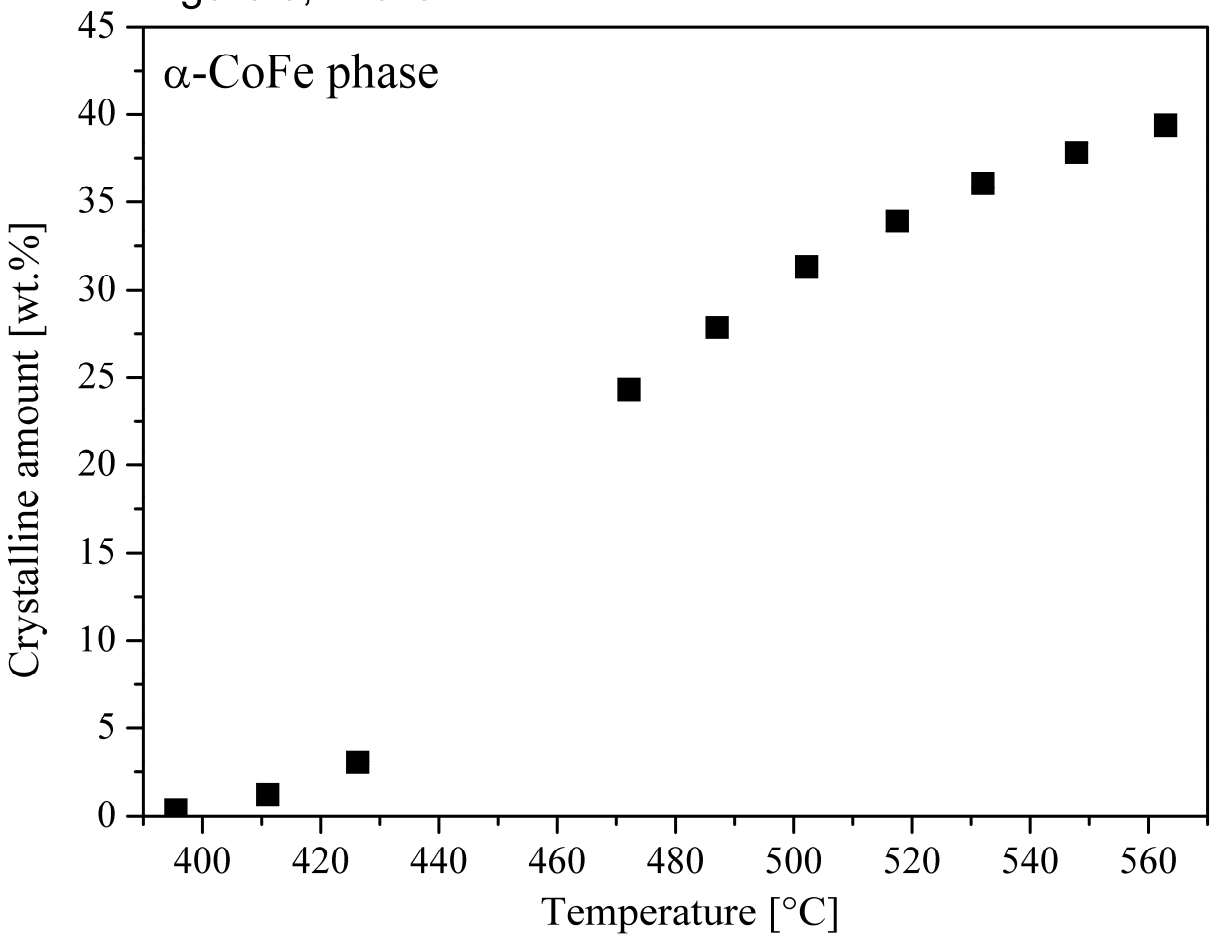

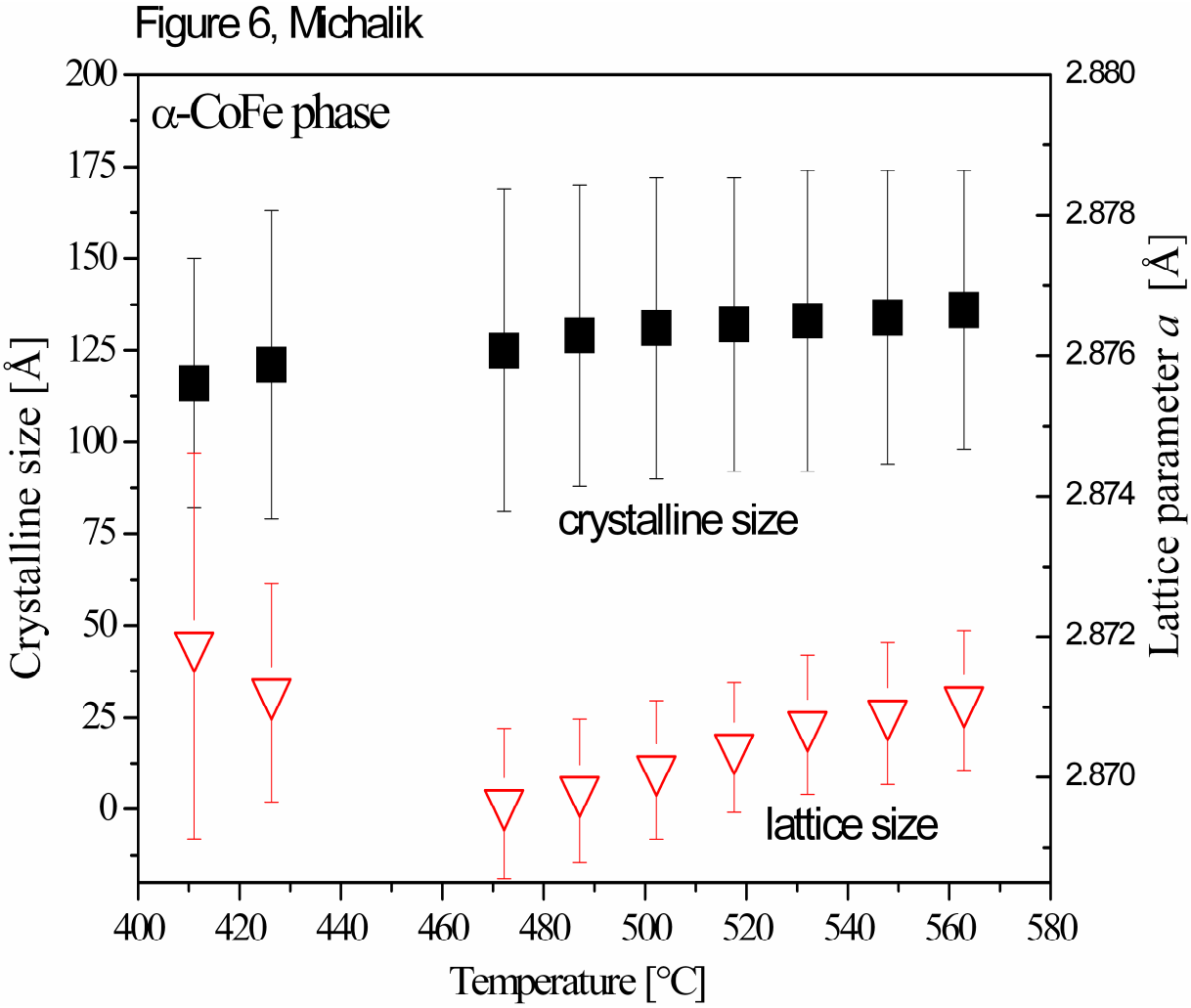
Figure 6, Michalik
α-CoFe phase
crystalline size
lattice size
Crystalline size [Å]
Lattice parameter a [Å]
Temperature [°C]
200
175
150
125
100
75
50
25
0
2.880
2.878
2.876
2.874
2.872
2.870
400
420
440
460
480
500
520
540
560
580

Figure 7, Michalik et al.